PPSD GAN: PPSD-informed Generative Model for Ambient Seismic Noise Synthesizing

Keunsuk Cho[†], Jeongun Ha[†], Jihun Lim[†], Jongwon Han[♯], Seongryong Kim[♭], and Donghun Lee[*]

***Abstract*—Extensive research has been conducted in the domain of seismic noise to enhance the quality of seismic signals. However, despite these efforts, a notable gap exists in the literature concerning the physical properties of seismic noise with rigorous quantitative assessment methodologies for its characterization. Therefore, we suggest our data-driven generative model PPSD GAN, unconditional WGAN-GP framework which is trained with the PPSD loss. We define a metric PPSD score for evaluation by leveraging the information contained in the PPSD histogram. We used two distinct datasets sampled from noisy and quiet areas in our study. Compared with previous approaches, PPSD GAN achieved 9.6-24.3% higher PPSD scores compared to the existing models in both regions. The waveform generated by PPSD GAN is visually similar to the actual waveform. Also, the experimental result shows that our model succeeded in learning the regional characteristics.**

***Index Terms*—Seismic Noise, Wasserstein GAN (WGAN-GP), Probabilistic Power Spectral Density (PPSD)**

I. Introduction

AMBIENT seismic noise, resulting from continuous ground vibrations, has been the subject of extensive investigation. There are multifaceted origins of seismic noise: microseism by ocean waves, wind-induced vibrations, vehicular and instrumental sources, and electrical interference [1]. The causes of seismic noise exhibit variability contingent on the vibration period, as elucidated by [2]. For instance, seismic noise shorter than 1-second period predominantly emanates from human-caused activities, including vehicular and machinery operations periods longer than that can be ascribed to the interaction of the vibrations with propagated underground structures [3], [4]. The uneven and transient distribution of these noise sources in time, space, and period result in non-stationary and non-linear seismic noise depending on the recorded location [5]. Consequently, to comprehensively analyze the different signals recorded in seismograms, it is essential to investigate the corresponding seismic noise within the specific monitoring area.

We aim to generate seismic noise signals based on data information. Seismic noise is predominantly associated with the analysis of seismic waveforms, where the process has conventionally been limited to noise decomposition based on physical models [6]. Data-driven noise generation can provide statistics or foundational data based on actual characteristics of the noise. In addition, it offers utility across a broader range of seismic applications. For instance, seismic noise leveraged to monitor subsurface phenomena such as [7], and [8] employed seismic noise to scrutinize Earth's crustal structure. From the deep-learning perspective, superposing white noise has been an appropriate way to augment the event signal [9]. But replacing the white noise with the real seismic noise signal is a promising way to augment the earthquake signals [10].

Due to the non-stationary and non-Gaussian randomness, adopting a physically meaningful quantitative metric is critical, we need a quantitative metric to analyze generated seismic noise compared to the real ones. We have succeeded in training a model capable of generating high-fidelity seismic noise by devising the Probabilistic Power Spectral Density (PPSD) as a quantitative metric for evaluation and a loss for model training. We use datasets from two distinct conditions to show that our model catches the characteristics of noise in each site. Also, we compare our model to the Gaussian random-based noise generation which is currently used for data augmentation in seismic tasks.

II. Related works

A. Seismic Waveform Generation

In recent times, there has been a surge in research endeavors dedicated to seismic waveform generation through the utilization of generative neural networks. A notable contribution in this domain can be found in the work of [11], where a deep convolutional GAN (DCGAN) was employed to synthesize seismic events and seismic noise waveforms. Additionally, [12] leveraged conditional GAN (CGAN) architecture to analyze Seismic Impedance, harnessing seismic waveforms as input data. In a related vein, [13] introduced a pioneering approach employing Wasserstein GAN with gradient penalty (WGAN-GP) enriched with three conditional variables: earthquake magnitude, hypocentral distance, and average shear-wave velocity of the top 30 m (VS30), to generate seismic waveforms. In this paper, we will call their model 'BBGAN (Broadband earthquake ground motion model using GAN)'.

BBGAN is comprised of a conditional generator and a conditional discriminator. The generator accepts standard Gaussian noise and conditional variables, yielding a three-component accelerometer waveform as output. Conversely, the discriminator evaluates the authenticity of input data. Both the generator and discriminator operate with earthquake

This research was funded by the Korea Meteorological Administration Research and Development Program under Grant KMI2021-01112.

[†*]Authors are with AI Math Laboratory under the Department of Mathematics, Korea University, Seoul 02841, Republic of Korea

[†]Authors contributed equally to this letter.

[♯]Author is with Earthquake Research Center under the Korea Institute of Geoscience and Mineral Resources, Daejeon 34132, Republic of Korea

[♭]Author is with Seismology Laboratory under the Department of Earth and Environment Science, Korea University, Seoul 02841, Republic of Korea

[*]Corresponding author: Donghun Lee (holy@korea.ac.kr)

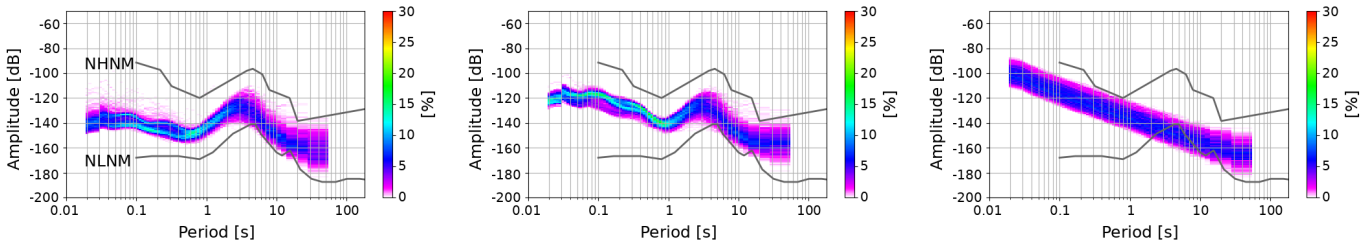

(a) Real (CHC2) (b) Real (SEO2) (c) White Noise

Fig. 1. PPSD plots from samples of (a) real CHC2 dataset, (b) real SEO2 dataset, and (c) white noise. The x-axis represents the period of the signal and the y-axis represents the amplitude of the signal. In the graph, the thick line at the top is NHNM and the thick line at the bottom is NLNM. Information about the histogram values is displayed in the right bar. It is clear that the white noise does not lie between the NLNM and HLNM, meaning that white noise is not appropriate as seismic noise.

magnitude, hypocentral distance, and VS30 as conditional variables. In this research, we decided to use BBGAN as a backbone model for our model.

B. Probabilistic Power Spectral Density (PPSD)

Seismic noise analysis conventionally entails the computation of the Power Spectral Density (PSD), which graphically illustrates the distribution of signal power across different frequency components. A model for generating seismic noise originating from sediment transport in river systems, which is introduced in [14], utilized PSD both in the development and evaluation of their model. When a PSD, as exemplified in [15], is provided, the generation of seismic noise becomes feasible through the specification of a random phase derived from the PSD. The PSD of seismic noise is bounded by empirically the New Low Noise Model (NLNM) and New High Noise Model (NHNM), which determined empirical statistics in [16].

Analysis of seismic noise can be extended by calculating various PSD profiles and subsequently constructing a probability density function that characterizes the likelihood of noise presence at specific points on the PSD plot [17]. This widely used approach, termed the Probabilistic Power Spectral Density (PPSD) plot, was employed for the analysis of seismic noise in the United States, as detailed in [4]. The overall plot of the NLNM, NHNM, and PPSD are drawn in Fig. 1.

III. PPSD Score & PPSD GAN

A. PPSD Score

In this section, we propose a new method called the PPSD Score based on the PPSD histogram. First, we explain the fundamental concepts of PPSD histogram and their notations. Then, we suggest the concept of a difference map. Finally, we construct the PPSD loss applied to evaluation and model training.

The visualization of PPSD plot is done on top of the 2-dimensional histogram. Let x be the number of periodic bins, y be the number of power bins, n be the number of waveforms used in the estimation of PPSD and $H \in \mathbb{R}^{y\times x}$ be the PPSD histogram. For each periodic bin, say i-th bin, there corresponds a Probability Mass Function (PMF) p_i, which is an i-th column of matrix H. Each PMF p_i represents the distribution of power for each i-th periodic domain. Since the PPSD histogram characterizes the regional features, we assume it is robust to the choice of samples.

The difference map M is a x-dimensional vector. The entry M_i of the vector indicates how different it is between the power distribution $p_i^1,\ p_i^2$ of two samples in i-th periodic bin. The exact calculation for the difference map is as follows:

$$M_i = d(p_i^1,\ p_i^2) \qquad (i = 1, 2, .., x), \tag{1}$$

where d is one of the metrics L1, L2, or Jensen–Shannon divergence (JS). Since the difference map reflects the sample's quality in terms of distinct periodic bins, in our work, we actively make use of this comprehensive information contained in the difference map.

Since seismic data is recorded for east, north, and vertical directions (so-called E, N, Z channels), 3 difference maps exist correspondingly. Therefore PPSD score is calculated by summing up all the entries in the L1 difference maps for all three channels. The exact calculation for the PPSD score is as follows:

$$s = -\sum_{c\in C}\sum_{i=1}^{x} M_i^c \quad for \quad C = \{E, N, Z\}. \tag{2}$$

The difference map contains for each channel, and for each periodic bin, how the sample generated by the generator is different from the real sample. So using such information contained in the difference map, the generator learns to reduce the difference map, allowing it to generate data similar to the real data.

The PPSD loss is a transformed form of the PPSD Score that can be applied to model training as a loss function. To get PPSD loss, we first calculate the PSD value of 3-channeled waveform as computed in [4] and get $\{P_i^{real}\}_{i=1}^n,\ \{P_i^{syn}\}_{i=1}^n \subset \mathbb{R}^{3\times x}$ for each of the normalized real, synthetic waveforms $\{X_i^{real}\}_{i=1}^n,\ \{X_i^{syn}\}_{i=1}^n$. After that, the PPSD loss is defined as:

$$\mathcal{L}_{PPSD} = \frac{1}{n}\sum_{i=1}^{n} L_{Huber}(\mathbf{M}\odot P_i^{real},\ \mathbf{M}\odot P_i^{syn}), \tag{3}$$

where $\odot$ is element-wise multiplication and $\mathbf{M} \in \mathbb{R}^{3\times x}$ is a matrix where its row corresponds to the difference map for

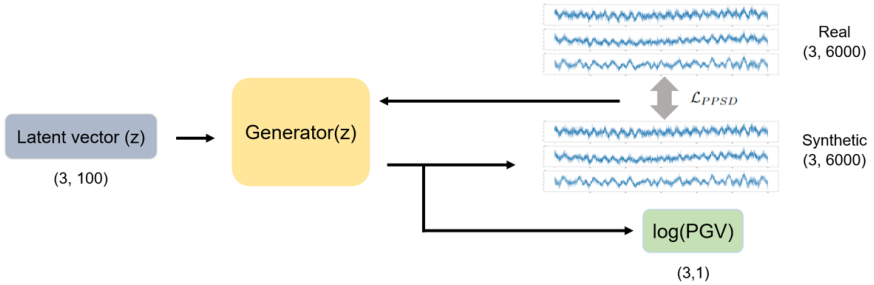

(a) Description of Generator for PPSD GAN

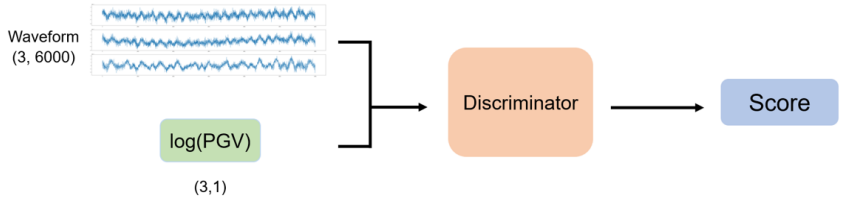

(b) Description of Discriminator for PPSD GAN

Fig. 2. The architectural framework of our model, can be summarized as follows: (a) The generator module receives a random Gaussian noise input denoted as 'z' and produces two distinct outputs — a normalized waveform and a vector labeled 'log(PGV)', signifying the scale of the waveforms. (b) Conversely, the discriminator module accepts input in the form of a waveform, 'log(PGV)' and subsequently yields a score.

each channel of the waveform. We choose Huber loss [18] as a regression loss since it is empirically optimal.

B. PPSD GAN

We propose our model, PPSD GAN, an unconditional WGAN-GP model which is an unconditional version of BB-GAN using PPSD loss. The detailed structure of the model is described in Fig. 2. For the generator loss, we added PPSD loss as mentioned in section III-A to better simulate the characteristics of the real samples. The loss functions used to train the generator and the discriminator of PPSD GAN are written as follows:

$$\begin{aligned}\mathcal{L}_D &= \mathbb{E}[D(G(Z))] - \mathbb{E}[D(X)] \\ &\quad + \lambda_{GP}\mathbb{E}[(\|\nabla_X D(X)\|_2 - 1)^2],\end{aligned} \tag{4}$$

$$\mathcal{L}_G = -\mathbb{E}[D(G(Z))] + \lambda_{PPSD}\mathcal{L}_{PPSD}, \tag{5}$$

where $\mathcal{L}_D$ is a discriminator loss, $\mathcal{L}_G$ is a generator loss, and $\mathcal{L}_{PPSD}$ is a PPSD loss. The random vector Z is a latent vector sampled from standard normal distribution and the random vector X is a tuple of normalized real waveform and the normalized logarithm of the Peak Ground Velocity (PGV) sample. The weights for gradient penalty and PPSD loss are written as λ_{GP} and λ_{PPSD}. Recall that by the choice of the distributional metric d, we can have a different choice of PPSD loss. In our experiment, we use three types of PPSD loss: L1, L2, and JS.

IV. Data & Method

A. Dataset

We conducted a comprehensive validation of our model's performance using data from two distinct field datasets. Each dataset is comprised of 1-minute waveforms with a response removal originating from two stations CHC2 and SEO2 (network code KS). These datasets were sampled meticulously to select noise from continuous 24-hour waveforms archived by the Korea Meteorological Administration (KMA) spanning the years 2016 to 2020.

Each dataset contains a substantial number of traces: CHC2 and SEO2 contain 12,340 and 11,514 traces, and was constructed with consistent sampling rates to ensure uniformity. This design allows for equitable subdivision based on criteria such as month, weekday, and time elapsed since noon, ensuring that each resulting sub-dataset maintains a similar size relative to the others. Additionally, to maintain data integrity, we systematically excluded any data recorded within a one-hour window of any of the reported local earthquakes in South Korea or global earthquakes with a magnitude exceeding 4.5, ensuring that all sampled traces exclusively represent noise data. All stations employed three-component broadband seismometers operating at a sampling rate of 100 Hz. Detailed PPSD plots for each station are provided in Fig. 1. The figure shows that SEO2, which corresponds to noisy areas, has remarkably higher levels and power in lower periods than in the CHC2. Basic information about CHC2 and SEO2 datasets is summarized in Table I.

TABLE I
Basic Information about Datasets

	CHC2	SEO2
Environments	Quiet	Noisy
Latitude	37.8	37.5
Longitude	127.9	126.9
Elevation (m)	268.0	114.0
Population Density (People / Km^2)	256	15,699

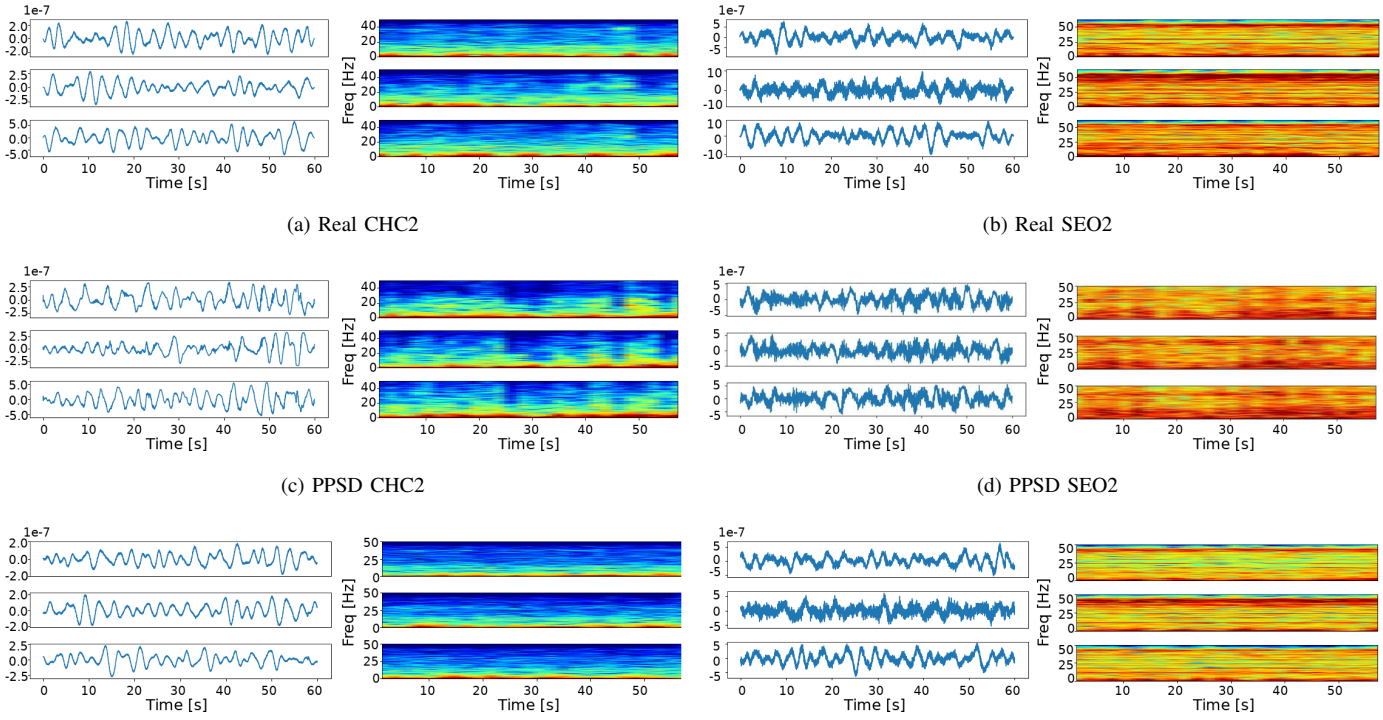

(a) Real CHC2

(b) Real SEO2

(c) PPSD CHC2

(d) PPSD SEO2

(e) PEX CHC2

(f) PEX SEO2

Fig. 3. Generated waveforms compared to real waveforms with spectrogram : (a) Real waveform of CHC2, (b) Real waveform of SEO2, (c) CHC2 waveform generated by PPSD GAN, (d) SEO2 waveform generated by PPSD GAN, (e) CHC2 waveform generated by PEX, and (f) SEO2 waveform generated by PEX.

B. Baseline

We adopt three baseline models, PSD Exploiter (PEX), white noise (WN) and BBGAN. WN adjusts the scale of the white noise signal by estimating the standard deviation from each of the waveforms in the real dataset. PEX is a noise generation technique that preserves the PSD to some extent. PEX takes the Fourier transform for a given noise, randomly mixes the phases, and then slices the signal obtained by taking the inverse Fourier transform to generate noise. Since our model adds the PPSD score to BBGAN, using BBGAN as a baseline can be seen as testing the case of $\lambda_{PPSD} = 0$.

C. Evaluation

We use the PPSD score to evaluate the synthetic sample generated by the models in general. To evaluate whether the sample resembles the real samples in the short periodic domain, we devise a Short Periodic Score (SPS) by tweaking a PPSD score. It is a summation of entries in a difference map only for a periodic component that is smaller than 1 sec. We specifically chose the threshold period as 1 sec considering the traits in noisy areas reported in [3], [4].

We use 92 periodic bins in the PPSD histogram and 42 bins to calculate SPS. Therefore the possible values of the PPSD score are between $-3 \times 92 \times 2 = -552$ and 0, whereas those of SPS are between $-3 \times 42 \times 2 = -252$ and 0. We normalize these raw PPSD and SPS scores between 0 and 1 for ease of comparison. The larger the number is, the better the synthetic samples are.

D. Implementation detail

For all models, we use a fixed batch size of 64 samples. We train the models using Adam optimizer with hyperparameter betas as $\beta_1 = 10^{-4}$ and $\beta_2 = 0.9$. We run all experiments with learning rates as 10^{-4} and weight for gradient penalty as 10. We train each model for 25 epochs on an NVIDIA RTX 3090 GPU.

V. Result

A. Waveform

As illustrated in Fig. 3, the waveform generated by the model trained with the PPSD score closely resembles the shape of real-world waveforms. This similarity is striking and is on par with, if not surpassing, the performance of PEX. The spectrogram results show that PEX fails to copy non-stationary waveform because it focuses only on matching the overall power content. On the other hand, our model can generate such a waveform.

B. PPSD plot and score

According to Table II, the best result of our model generates better samples than the baseline model does in terms of PPSD score. We can also see empirically that choosing L1 distance as the distributional distance is the optimal choice. As shown in Fig. 4, the PPSD plot derived from our model's sample matches well with that from the real dataset, compared to the method of the PEX. Moreover, we can see our model is especially outperforming other baseline models in terms of SPS.

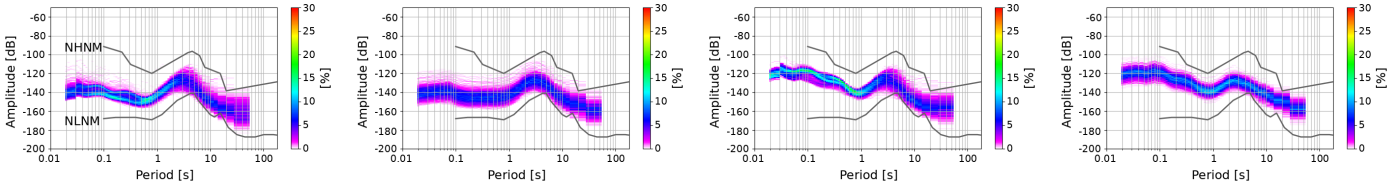

(a) Real (CHC2) (b) Ours (CHC2) (c) Real (SEO2) (d) Ours (SEO2)

Fig. 4. PPSD plots from samples of (a) real CHC2 dataset, (b) real SEO2 dataset, (c) CHC2 dataset generated by PPSD GAN, and (d) SEO2 dataset generated by PPSD GAN. The model reflects to some extent the difference in amplitude of noise generated in each of the two regions.

TABLE II
COMPARISON OF NORMALIZED PPSD SCORE AND SPS

Methods	PPSD (↑)		SPS (↑)	
	CHC2	SEO2	CHC2	SEO2
WN	0.277	0.417	0.013	0.372
PEX	0.662	0.585	0.540	0.398
BBGAN	0.676	0.759	0.617	0.698
Ours (L1)	**0.758**	**0.760**	**0.783**	**0.728**
Ours (L2)	0.677	0.649	0.544	0.622
Ours (JS)	0.710	0.743	0.696	0.672

VI. DISCUSSION

The waveforms generated by PPSD GAN seems to be quite similar to real seismic noise, capturing the different characteristics of noisy and quiet regions. Moreover, we can see our model is especially outperforming in predicting short-period signals based on analysis by SPS. Therefore, we can conclude that our model is capable of generating ambient noise reflecting the regional properties.

However, the waveform generated by our model trained with a noisy dataset generates unlikely samples that contain many peaks. We think that this phenomenon can be attributed to the model's capacity to capture the effects of short-period waves since this phenomenon is mostly observed in noisy cases.

It is also worth noting that unlike in PEX, PPSD GAN generates non-stationary seismic noise depending on the time window, which can be seen Fig. 3c-3d. So, our model is capable of generating diverse possible signals that could occur.

VII. CONCLUSION

In this letter, we employ the WGAN-GP framework to develop a model that generates ambient seismic noises in a station-wise manner. Additionally, we utilize a quantitative metric PPSD score to facilitate both training and evaluation of our model. Through our experimental observations, we find that the model adeptly captures the variations in waveforms attributed to differences in monitoring stations. It also achieved 9.6-24.3% higher PPSD scores compared to the baseline models in both regions. We firmly believe that our model possesses multifaceted utility, extending beyond waveform augmentation, to contribute to a spectrum of seismic tasks, including the enrichment of data for enhanced false alarm detection.

REFERENCES

[1] W. Zhu, S. M. Mousavi, and G. C. Beroza, "Seismic signal denoising and decomposition using deep neural networks," *IEEE Transactions on Geoscience and Remote Sensing*, vol. 57, no. 11, pp. 9476–9488, 2019.
[2] P. Bormann and E. Wielandt, "Seismic signals and noise," in *New Manual of Seismological Observatory Practice 2 (NMSOP2)*, P. Bormann, Ed. Potsdam: Deutsches GeoForschungsZentrum GFZ, 2013, pp. 1–62.
[3] F. Ringdal and H. Bungum, "Noise level variation at norsar and its effect on detectability," *Bulletin of the Seismological Society of America*, vol. 67, no. 2, pp. 479–492, 1977.
[4] D. E. McNamara and R. P. Buland, "Ambient noise levels in the continental united states," *Bulletin of the seismological society of America*, vol. 94, no. 4, pp. 1517–1527, 2004.
[5] T. Zhong, Y. Li, N. Wu, P. Nie, and B. Yang, "Statistical properties of the random noise in seismic data," *Journal of applied Geophysics*, vol. 118, pp. 84–91, 2015.
[6] Y. Chen, "Non-stationary least-squares complex decomposition for microseismic noise attenuation," *Geophysical Journal International*, vol. 213, no. 3, pp. 1572–1585, 2018.
[7] O. Méric, S. Garambois, J.-P. Malet, H. Cadet, P. Gueguen, and D. Jongmans, "Seismic noise-based methods for soft-rock landslide characterization," *Bulletin de la Société Géologique de France*, vol. 178, no. 2, pp. 137–148, 2007.
[8] N. M. Shapiro, M. Campillo, L. Stehly, and M. H. Ritzwoller, "High-resolution surface-wave tomography from ambient seismic noise," *Science*, vol. 307, no. 5715, pp. 1615–1618, 2005.
[9] S. M. Mousavi, W. L. Ellsworth, W. Zhu, L. Y. Chuang, and G. C. Beroza, "Earthquake transformer—an attentive deep-learning model for simultaneous earthquake detection and phase picking," *Nature communications*, vol. 11, no. 1, p. 3952, 2020.
[10] W. Zhu, S. M. Mousavi, and G. C. Beroza, "Seismic signal augmentation to improve generalization of deep neural networks," in *Advances in geophysics*. Elsevier, 2020, vol. 61, pp. 151–177.
[11] T. Wang, D. Trugman, and Y. Lin, "Seismogen: Seismic waveform synthesis using generative adversarial networks," *arXiv preprint arXiv:1911.03966*, 2019.
[12] D. Meng, B. Wu, Z. Wang, and Z. Zhu, "Seismic impedance inversion using conditional generative adversarial network," *IEEE Geoscience and Remote Sensing Letters*, vol. 19, pp. 1–5, 2021.
[13] M. A. Florez, M. Caporale, P. Buabthong, Z. E. Ross, D. Asimaki, and M.-A. Meier, "Data-driven synthesis of broadband earthquake ground motions using artificial intelligence," *Bulletin of the Seismological Society of America*, vol. 112, no. 4, pp. 1979–1996, 2022.
[14] V. C. Tsai, B. Minchew, M. P. Lamb, and J.-P. Ampuero, "A physical model for seismic noise generation from sediment transport in rivers," *Geophysical Research Letters*, vol. 39, no. 2, 2012.
[15] Y. Ban and J.-S. Yang, "Layout aware line-edge roughness modeling and poly optimization for leakage minimization," in *Proceedings of the 48th Design Automation Conference*, 2011, pp. 447–452.
[16] J. R. Peterson, "Observations and modeling of seismic background noise," U.S. Geological Survey, Reston, VA, USA, Tech. Rep. 93-322, 1993.
[17] D. E. McNamara and R. Boaz, *Seismic noise analysis system using power spectral density probability density functions: A stand-alone software package*. Reston, VA, USA: US Geological Survey, 2006.
[18] K. Gokcesu and H. Gokcesu, "Generalized huber loss for robust learning and its efficient minimization for a robust statistics," *arXiv preprint arXiv:2108.12627*, 2021.